Quantitative model of electron energy loss in XPS

A. Cohen Simonsen
Department of Physics, University of Odense, DK-5230 Odense M, Denmark

F. Yubero
Instituto de Ciencia de Materiales de Sevilla, University of Sevilla, 41092 Sevilla, Spain

S. Tougaard
Department of Physics, University of Odense, DK-5230 Odense M, Denmark

(Received 16 December 1996)

A model for the inelastic-scattering cross section of electrons in XPS experiments is presented. The calculation is analogous to a previous model for reflection-electron energy-loss spectroscopy by Yubero *et al.* [Phys. Rev. B **53**, 9719 (1996)]. The model treats the general case of photoelectron creation at arbitrary depth and with arbitrary exit angle and electron energy. The effect of the core hole as well as surface effects are included in the model. We study systematically the behavior of the model when the energy, exit angle, and depth of origin are varied. Furthermore, the effect of the core hole on the energy loss is investigated in detail. The results are compared with experimental XPS spectra from aluminum metal. [S0163-1829(97)01127-2]

I. INTRODUCTION

Surface electron spectroscopies such as XPS (x-ray photoelectron spectroscopy), AES (Auger electron spectroscopy), and REELS (reflection-electron energy-loss spectroscopy) are highly influenced by inelastic-scattering events experienced by electrons. Thus, for the purpose of quantification a thorough understanding of the energy loss is important.

The usual quantity employed to describe the energy loss is the inelastic cross section, which gives the probability density per unit path length of losing the energy $\hbar\omega$. It can be expressed in terms of the complex dielectric function $\epsilon(\mathbf{k},\omega)$ of the particular medium, and for electrons traveling in an infinite medium it is given by[1,2]

$$K(E_0,\hbar\omega)=\frac{1}{E_0\pi a_0}\int_{k_-}^{k_+}\frac{dk}{k}\,\mathrm{Im}\left[\frac{1}{\epsilon(k,\omega)}\right], \qquad (1)$$

where the following quantities are introduced: E_0 is the initial energy of the electron, a_0 is the Bohr radius, and k is the wave vector transferred from the electron. $k_\pm=(2m/\hbar^2)^{1/2}[E_0^{1/2}\pm(E_0-\hbar\omega)^{1/2}]$ are the limits on the k vector imposed by energy and momentum conservation during the inelastic scattering. This model, however, does not reproduce the surface loss features observed in REELS and XPS. Attempts have been made to model the inelastic cross section as a linear combination of $\mathrm{Im}[1/\epsilon]$ and $\mathrm{Im}[1/(1+\epsilon)]$.[3] Although a reasonable fit to experiment can be made, the values of the fitting parameters seem unphysical and inconsistent.

A more realistic model for REELS has been developed to describe the electron energy loss for normal incidence and exit geometry.[4] It treats the total transport process for an electron elastically backscattered a certain depth below the surface. The model was recently extended to include general incidence and exit angles[5] and was compared to experimental inelastic cross sections[6] deconvoluted from experimental REELS spectra. The quantitative agreement regarding the dependence on incidence and exit angle as well as on initial energy was good and all the main loss features of the experiment were reproduced.

The purpose of the present paper is to take a similar approach to the case of XPS. The system was previously studied by Gervasoni and Arista[7] who determined the energy-loss rate, but not the energy-loss distribution, i.e., the cross section. Seymour *et al.*[8] modeled the plasmon loss intensity in photoemission on the basis of a hydrodynamical equation. However, the model produced spurious structures in the losses that was not reproduced experimentally. Recently Chen and Chen proposed a model that incorporates both surface and bulk losses into the Landau formula for the energy distribution.[9] This procedure however, has three main weaknesses: First, they integrate the surface loss function over all depths; i.e., they assume that the contribution from surface losses is the same for an electron excited at the surface and one excited deep in the bulk. Second, they incorporate this path-integrated surface loss function directly into the Landau formula. This implies that they allow for multiple surface losses to infinite order. Third, they ignore the effect of the core hole on the energy loss of the photoelectron. The first two procedures are not properly justified and the last approximation is shown in the present work not to hold.

We treat the general case of photoelectron creation at arbitrary depth and with arbitrary exit angle of the electron. The procedure is based on the ''specular reflection model,'' [7,10] which allows one to solve the electrodynamic problem with the proper boundary conditions. The result is expressed in terms of the effective inelastic cross section giving the energy-loss distribution for the total photoemission process.

II. THEORY

We consider the following situation as a model of the experimental XPS process, Fig. 1(a): a semi-infinite medium

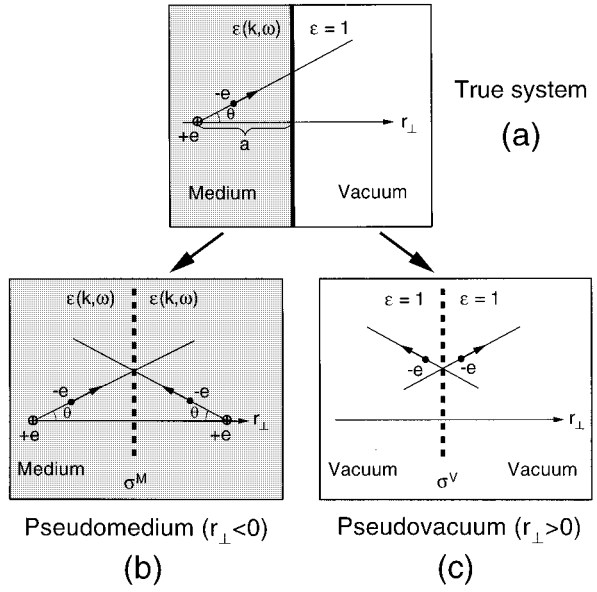

FIG. 1. Geometry of the hole and electron in the true experimental XPS system (a). The equivalent pseudomedium (b) and pseudovacuum (c) that has been used in the calculation of K_{eff}.

with dielectric function $\epsilon(\mathbf{k},\omega)$ occupying the half space $r_\perp<0$, and a vacuum region with $\epsilon=1$ occupying $r_\perp>0$. At time $t=0$ an electron-hole pair is created at depth a below the surface. The electron moves in a straight line with velocity $\mathbf{v}=(v_\perp,v_\parallel)$, energy $E_0=\frac{1}{2}mv^2$, and angle θ to the surface normal, while the core hole is stationary. At time $t_s=a/v_\perp$ the electron crosses the surface and leaves the solid. We assume constant velocity of the electron. This approximation is only valid when the energy loss $\hbar\omega$ is negligible compared to E_0. The electron-hole pair creates an induced charge density in the medium during photoexcitation and electron transport. The origin of the electron energy loss is that the electric field induced in the medium acts on the electron as it moves. In accordance with previous considerations[4,5] it is possible to express an effective inelastic cross section $K_{\mathrm{eff}}(E_0,\hbar\omega,a,\theta)$ in terms of the induced potential. This is defined as the average probability that an electron shall lose energy $\hbar\omega$ per unit energy loss and unit path length while traveling in the specified geometry. The average is over the path length traveled in the solid $x=a/\cos(\theta)$. Clearly, this has to be integrated over path lengths to be compared with experimental XPS. K_{eff} is given by

$$K_{\mathrm{eff}}(E_0,\hbar\omega,x)=\frac{2}{(2\pi)^4 x\hbar^2\omega}\int_{-\infty}^{\infty}dt\int d^3r\ \rho_e(\mathbf{r},t)\times\mathrm{Re}\left[i\int d^3k\ \mathbf{k}\cdot\mathbf{v}\Phi_{\mathrm{ind}}(\mathbf{k},\omega)e^{i\mathbf{k}\cdot\mathbf{r}-i\omega t}\right], \tag{2}$$

where $\rho_e(\mathbf{r},t)$ is the charge density of the electron and $\Phi_{\mathrm{ind}}(\mathbf{k},\omega)$ is the induced potential, determined from the total potential by the relation $\Phi_{\mathrm{ind}}(\mathbf{k},\omega)=\Phi(\mathbf{k},\omega)-\Phi(\mathbf{k},\omega)|_{\epsilon=1}$.[7] Equation (2) describes the probability for the electron to interact with the particular frequency component $\Phi_{\mathrm{ind}}(\omega)$ of the induced potential, where Φ_{ind} is created by the hole and the electron itself. Now the primary objective is to find $\Phi(\mathbf{k},\omega)$ in the two half spaces (medium and vacuum) of the system, i.e., to solve Poisson's equation. To this purpose, the ''specular reflection model'' has proven useful in the case of REELS (Refs. 4 and 5) and XPS (Ref. 7). The medium and the vacuum are treated separately in two infinite pseudomedia M [Fig. 1(b)] and V [Fig. 1(c)]. The relevant charges are the electron ρ_e, the core hole ρ_h, their images $\rho_{e'}$, $\rho_{h'}$, and fictitious surface charges σ^M, σ^V introduced to satisfy the boundary conditions. The charge densities are expressed as

$$\rho_e(\mathbf{r},t)=-e\,\delta(\mathbf{r}-\mathbf{a}-\boldsymbol{\nu}t),\quad t>0,$$

$$\rho_{e'}(\mathbf{r},t)=-e\,\delta(\mathbf{r}+\mathbf{a}-\boldsymbol{\nu}'t),\quad t>0,$$

$$\rho_h(\mathbf{r},t)=e\,\delta(\mathbf{r}-\mathbf{a}),\quad t>0,$$

$$\rho_{h'}(\mathbf{r},t)=e\,\delta(\mathbf{r}+\mathbf{a}),\quad t>0,$$

$$\rho_e(\mathbf{r},t)=\rho_{e'}(\mathbf{r},t)=\rho_h(\mathbf{r},t)=\rho_{h'}(\mathbf{r},t)=0,\quad t<0, \tag{3}$$

where $\mathbf{v}=(v_\perp,v_\parallel)$, $\mathbf{v}'=(-v_\perp,v_\parallel)$, $\mathbf{a}=(-a,0)$. Poisson's equation in Fourier space for each of the two infinite pseudomedia is

$$\Phi^M(\mathbf{k},\omega)=\frac{4\pi}{k^2\epsilon(\mathbf{k},\omega)}[\rho^M_{ee'}(\mathbf{k},\omega)+\rho^M_{hh'}(\mathbf{k},\omega)+\sigma^M(k_\parallel,\omega)], \tag{4}$$

$$\Phi^V(\mathbf{k},\omega)=\frac{4\pi}{k^2}[\rho^V_{ee'}(\mathbf{k},\omega)+\sigma^V(k_\parallel,\omega)]. \tag{5}$$

The Fourier-transformed charge densities $\rho^M_{ee'}(\mathbf{k},\omega)$, $\rho^M_{hh'}(\mathbf{k},\omega)$ and $\rho^V_{ee'}(\mathbf{k},\omega)$ are evaluated in the time intervals where the electron travels in the medium and vacuum, respectively:

$$\rho^M_{ee'}(\mathbf{k},\omega)=\int_0^{t_s}dt\int d^3r[\rho_e(\mathbf{r},t)+\rho_{e'}(\mathbf{r},t)]e^{-i\mathbf{k}\cdot\mathbf{r}+i\omega t},$$

$$\rho^M_{hh'}(\mathbf{k},\omega)=\int_0^{\infty}dt\int d^3r[\rho_h(\mathbf{r},t)+\rho_{h'}(\mathbf{r},t)]e^{-i\mathbf{k}\cdot\mathbf{r}+i\omega t},$$

$$\rho^V_{ee'}(\mathbf{r},t)=\int_{t_s}^{\infty}dt\int d^3r[\rho_e(\mathbf{r},t)+\rho_{e'}(\mathbf{r},t)]e^{-i\mathbf{k}\cdot\mathbf{r}+i\omega t}. \tag{6}$$

Application of the electromagnetic boundary conditions $\Phi^V(r_\perp=0^+)=\Phi^M(r_\perp=0^-)$ and $\partial\Phi^V/\partial r_\perp(r_\perp=0^+)=\epsilon\partial\Phi^M/\partial r_\perp(r_\perp=0^-)$ to Eqs. (4) and (5) will determine the fictitious surface charges $\sigma^M(k_\parallel,\omega)$ and $\sigma^V(k_\parallel,\omega)$. The result is $\sigma^V(k_\parallel,\omega)=-\sigma^M(k_\parallel,\omega)=\sigma(k_\parallel,\omega)$, where

$$\sigma(k_\parallel,\omega)=\frac{2}{1+\epsilon}\,(F^M_{ee'}+F^M_{hh'})-\frac{2\epsilon}{1+\epsilon}\,F^V_{ee'}, \tag{7}$$

and $F^M_{ee'}$, $F^M_{hh'}$, $F^V_{ee'}$ are defined as

$$F^M_{ee'}(k_\parallel,\omega)=\frac{k_\parallel}{2\pi}\int_{-\infty}^{\infty}\frac{\rho^M_{ee'}(\mathbf{k},\omega)}{k_\perp^2+k_\parallel^2}\,dk_\perp =\frac{ie}{\nu_\perp}\left(\frac{e^{i\Omega_0 a}-e^{-k_\parallel a}}{\Omega_0-ik_\parallel}\right), \tag{8}$$

$$F^M_{hh'}(k_\parallel,\omega)=\frac{k_\parallel}{2\pi}\int_{-\infty}^{\infty}\frac{\rho^M_{hh'}(\mathbf{k},\omega)}{k_\perp^2+k_\parallel^2}\,dk_\perp =e\left(\pi\delta(\omega)+\frac{i}{\omega}\right)e^{-k_\parallel a}, \tag{9}$$

$$F^V_{ee'}(k_\parallel,\omega)=\frac{k_\parallel}{2\pi}\int_{-\infty}^{\infty}\frac{\rho^V_{ee'}(\mathbf{k},\omega)}{k_\perp^2+k_\parallel^2}\,dk_\perp=\frac{-ie}{\nu_\perp}\left(\frac{e^{i\Omega_0 a}}{\Omega_0+ik_\parallel}\right) \tag{10}$$

and $\Omega_0=(\omega-k_\parallel v_\parallel)/v_\perp$

Equation (7) implies that the dielectric function satisfies the constraint $\epsilon(\mathbf{k},\omega)=\epsilon(k_\parallel,\omega)$. The validity of this approximation was discussed previously.[5] Now the induced potential is found from the total potential as

$$\Phi^M_{\rm ind}(\mathbf{k},\omega)=\frac{4\pi}{k^2}\left[\left(\frac{1}{\epsilon}-1\right)(\rho^M_{ee'}(\mathbf{k},\omega)+\rho^M_{hh'}(\mathbf{k},\omega))+\frac{(\epsilon-1)(\epsilon+2)}{\epsilon(\epsilon+1)}\,(F^M_{ee'}+F^M_{hh'})+\frac{(1-\epsilon)}{(1+\epsilon)}\,F^V_{ee'}\right], \tag{11}$$

$$\Phi^V_{\rm ind}(\mathbf{k},\omega)=\frac{4\pi}{k^2}\,\frac{(1-\epsilon)}{(1+\epsilon)}\,(F^M_{ee'}+F^M_{hh'}+F^V_{ee'}). \tag{12}$$

Substitution of Eqs. (8)–(12) into Eq. (2) gives the effective inelastic cross section $K_{\rm eff}(E_0,\hbar\omega,a,\theta)$. Integration in space and time is straightforward, remembering that $\Phi^M_{\rm ind}(\mathbf{k},\omega)$ must be used for $0<t<t_s$ and $\Phi^V_{\rm ind}(\mathbf{k},\omega)$ for $t>t_s$. Analytical integration in k space is not possible with the proper limits from momentum and energy conservation. However, with cylindrical coordinates ($d^3k=2\pi k_\parallel dk_\parallel dk_\perp$) and the approximation of extending the limits of $k_\perp$ to $-\infty<k_\perp<\infty$ it is possible to perform the $k_\perp$ integration analytically. As previously noted[5] this approximation is not expected to give large errors. With extensive use of Cauchy's residue theorem and substitution of the expressions for $F^M_{ee'}$, $F^M_{hh'}$ and $F^V_{ee'}$, $K_{\rm eff}$ is finally found as a sum of four terms, $K_{\rm eff}(E_0,\hbar\omega,a,\theta)=K_{M1}+K_{M2}+K_{M3}+K_V$, where

$$K_{M1}=\frac{\cos\theta}{\pi a_0 E_\perp}\,{\rm Re}\left[i\int k_\parallel dk_\parallel\,\frac{(1/\epsilon-1)}{\Omega_0^2+k_\parallel^2}\right]+\frac{-1}{2\pi E_\perp a_0 x\omega_\perp}\,{\rm Re}\left[i\int k_\parallel dk_\parallel\,\frac{(1/\epsilon-1)}{(\Omega_0^2+k_\parallel^2)^2}\left\{\left(i+\frac{\nu_\parallel}{\nu_\perp}\right)(\Omega_0+ik_\parallel)^2(e^{-i\Omega_0 a-k_\parallel a}-1)\right.\right.$$
$$\left.\left.+\left(-i+\frac{\nu_\parallel}{\nu_\perp}\right)(\Omega_0-ik_\parallel)^2(e^{i\Omega_0 a-k_\parallel a}-1)+\left(i-\frac{\nu_\parallel}{\nu_\perp}\right)(e^{-i\Omega_0 a}-e^{-k_\parallel a})(e^{i\Omega_0 a}-e^{-k_\parallel a})(\Omega_0^2+k_\parallel^2)\right\}\right], \tag{13}$$

$$K_{M2}=\frac{-1}{2\pi E_\perp a_0 x\omega_\perp}\,{\rm Re}\left[\left(\pi\delta(\omega_\perp)+\frac{i}{\omega_\perp}\right)\int k_\parallel dk_\parallel\,\frac{(1/\epsilon-1)}{\Omega_0^2+k_\parallel^2}\left\{\left(i+\frac{\nu_\parallel}{\nu_\perp}\right)(\Omega_0+ik_\parallel)(1-e^{-k_\parallel a-i\Omega_0 a})\right.\right.$$
$$\left.\left.+\left(-i+\frac{\nu_\parallel}{\nu_\perp}\right)(\Omega_0-ik_\parallel)(e^{-2k_\parallel a}-e^{-k_\parallel a-i\Omega_0 a})\right\}\right], \tag{14}$$

$$K_{M3}=\frac{-1}{2\pi E_\perp a_0 x\omega_\perp}\,{\rm Re}\left[i\int k_\parallel dk_\parallel\,\frac{(-i+\nu_\parallel/\nu_\perp)(\Omega_0-ik_\parallel)(e^{-k_\parallel a}-e^{-i\Omega_0 a})}{\Omega_0^2+k_\parallel^2}\left\{\frac{(\epsilon-1)(\epsilon+2)}{\epsilon(\epsilon+1)}\left[(e^{i\Omega_0 a}-e^{-k_\parallel a})\left(\frac{\Omega_0+ik_\parallel}{\Omega_0^2+k_\parallel^2}\right)\right.\right.\right.$$
$$\left.\left.\left.-i\left(\pi\delta(\omega_\perp)+\frac{i}{\omega_\perp}\right)e^{-k_\parallel a}\right]+\frac{(\epsilon-1)}{(\epsilon+1)}\left(\frac{\Omega_0-ik_\parallel}{\Omega_0^2+k_\parallel^2}\right)e^{i\Omega_0 a}\right\}\right], \tag{15}$$

$$K_V=\frac{1}{2\pi E_\perp a_0 x\omega_\perp}\,\mathrm{Re}\left[\int k_\parallel dk_\parallel\,\frac{(1-\epsilon)}{(1+\epsilon)}\,\frac{(1-i\nu_\parallel/\nu_\perp)(\Omega_0+ik_\parallel)e^{-i\Omega_0 a}}{\Omega_0^2+k_\parallel^2}\left\{\frac{2ik_\parallel e^{i\Omega_0 a}-(\Omega_0+ik_\parallel)e^{-k_\parallel a}}{\Omega_0^2+k_\parallel^2}\right.\right.$$
$$\left.\left.-i\left(\pi\delta(\omega_\perp)+\frac{i}{\omega_\perp}\right)e^{-k_\parallel a}\right\}\right], \tag{16}$$

and $E_\perp=\frac{1}{2}mv_\perp^2$ and $\omega_\perp=\omega/v_\perp$. Of the four terms above, K_{M1}, K_{M2}, and K_{M3} correspond to losses inside the medium, while K_V describes losses outside. The limits of the integrals in Eqs. (13)–(16) are found by setting $k^2=k_\parallel^2+\Omega_0^2$ and solving for $k_\parallel$. The result is

$$k_{\parallel\pm}=\frac{\omega\nu_\parallel}{\nu^2}+\left[\frac{\nu_\perp^2}{\nu^2}\left(k_\pm^2-\frac{\omega^2}{\nu^2}\right)\right]^{1/2}. \tag{17}$$

In the limit of $a\to\infty$, K_{eff} reduces to the first term of Eq. (13). This is equal to the limit obtained with the effective cross section for REELS (Ref. 5) when $\theta_i=\theta_0=\theta$. For $\theta=0$ this limit equals the inelastic cross section for electrons in an infinite medium, i.e., Eq. (1). However, this is not the case for larger angles. This shortcoming might be due to the approximation of the $k_\perp$ integration limits. Despite the fact that the problem was also found in REELS,[5] this model showed good agreement with experiment. The correctness of the model can be tested when comparing the XPS cross section with model $A+$ in Ref. 4. For this purpose we must set $\theta=0$ and remove the core hole from the new model. Removing the core hole is simple since all terms related to it contain the factor $[\pi\delta(\omega_\perp)+i/\omega_\perp]$. When this is carried out, we obtain an exact match between the new model and the old model $A+$ for all values of E_0 and a. That is, the new model for XPS is consistent with the previous model for REELS. The effective inelastic cross section gives information on the energy loss of photoelectrons originating from the depth a below the surface. But experimental XPS spectra sample electrons from a whole range of depths. This implies that one should perform a suitable integration of K_{eff} over path lengths to make it comparable with experiment. In the previous work on REELS this was done according to the expression[4,5]

$$K_{\mathrm{sc}}(E_0,\hbar\omega,\theta)=\int_0^\infty\frac{x}{\lambda^2}\,e^{-x/\lambda}K_{\mathrm{eff}}(E_0,\hbar\omega,\theta,a)dx, \tag{18}$$

where $x=a/\cos\theta$ and elastic scattering is neglected. It must be considered, though, whether this is also a valid procedure for XPS.

It is common practice to divide the energy loss in XPS into intrinsic and extrinsic losses.[11,12] The first are related to the sudden creation of the electron-hole pair at $t=0$, while the latter are produced during transport of the electron through the medium. Since the intrinsic excitations occur only at time $t=0$ they contribute to the effective cross section per unit path length as K_{intr}/x. Therefore we can divide K_{eff} into two terms, $K_{\mathrm{eff}}=K_{\mathrm{intr}}/x+K_{\mathrm{extr}}$, where K_{intr} and K_{extr} give the contributions from intrinsic and extrinsic losses, respectively. Substitution into Eq. (18) results in attenuation of the intrinsic part as $K_{\mathrm{intr}}e^{-x/\lambda}$ and attenuation of the extrinsic part as $K_{\mathrm{extr}}xe^{-x/\lambda}$ as expected. It is important to notice, however, that in XPS the inelastic cross section calculated according to Eq. (18) describes only the first inelastic scattering event. It cannot serve to model the full spectrum (by repeated convolution) since it contains the intrinsic part of the energy loss, which is inseparable from the rest.

From the derivations in Ref. 13 we can determine the model spectrum corresponding to one inelastic scattering event:

$$J(E)\propto\cos(\theta)\left[F(E)+\lambda\int_E^\infty dE'F(E')K_{sc}(E_0,E'-E,\theta)\right], \tag{19}$$

where $F(E)$ is the primary excitation spectrum modeled with a Lorentzian. The inelastic mean free path λ is taken from the literature[14] and is assumed independent of a.

III. RESULTS

We have studied how the loss features of K_{eff} and K_{sc} vary when the parameters a, E_0, and θ change. As a model dielectric function $\epsilon(\mathbf{k},\omega)$ we use the simple result for aluminum Eq. (20), with k dependence introduced according to Ritchie and Howie:[15]

$$\epsilon(\mathbf{k},\omega)=1-\frac{\omega_p^2}{\omega^2-\omega_k^2+i\gamma_0\omega},\quad \hbar\omega_k=\frac{\hbar^2k^2}{2m}. \tag{20}$$

Here $\hbar\omega_p=15.6$ eV and $\hbar\gamma_0$ is given in Table I.[4]

Figure 2 shows the exit-angle dependence of $K_{\mathrm{eff}}(E_0,\hbar\omega,a,\theta)$ with fixed primary energy ($E_0=1000$ eV) and excitation depth ($a=10$ Å). The bulk and surface plasmons are clearly identified at 15.6 and 11.0 eV, respectively. For growing exit angles there is an increase in the surface-to-bulk ratio as expected. In addition the overall cross section decreases with increasing exit angle because the path length in the medium increases. This is the explanation for the decrease in the surface plasmon intensity in going from 60° to 70°.

Figure 3 gives the dependence of $K_{\mathrm{eff}}(E_0,\hbar\omega,a,\theta)$ on the excitation depth a, with fixed exit angle ($\theta=0°$) and energy ($E_0=1000$ eV). The relative importance of the surface plas-

TABLE I. Values for Al of the parameter $\hbar\gamma_0$ used in Eq. (20) for calculation of the dielectric function.

E_0 (eV)	175	300	500	1180	2000
$\hbar\gamma_0$ (eV)	3.4	2.8	2.1	1.5	1.3

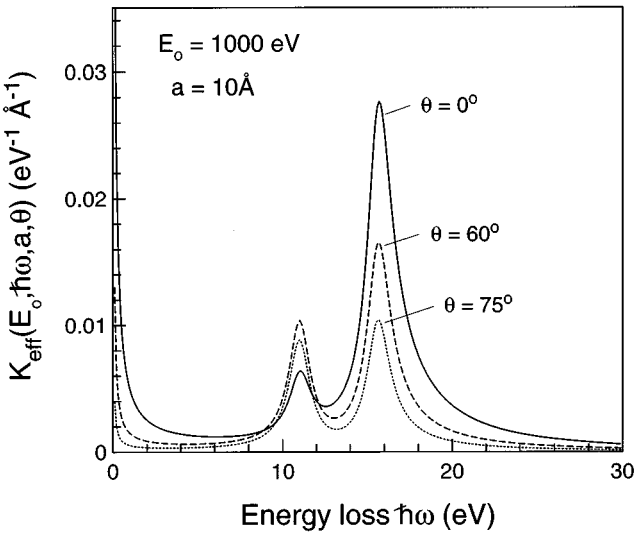

FIG. 2. Exit angle dependence of the effective inelastic cross section K_{eff} in aluminum. The angles $\theta=0°$, 60°, and 75° where considered. The energy $E_0=1000$ eV and depth of excitation $a=10$ Å are fixed.

mon is diminished when large depths are considered. This is caused by the larger time the electron spends in the bulk compared with the surface region. In addition, the figure demonstrates how $K_{\text{eff}}(E_0,\hbar\omega,a,\theta)$ approaches the infinite medium result [Eq. (1)] for $a\rightarrow\infty$. Notice that there is an overall increase in K_{eff} with decreasing a. The reason for this is that the relative importance of the intrinsic losses and the losses in vacuum increases as a approaches zero.

Figures 4(a) and 4(b) show the energy dependence of $K_{\text{eff}}(E_0,\hbar\omega,a,\theta)$ for fixed excitation depth and exit angle ($\theta=0°$). At $a=200$ Å there is an overall attenuation of K_{eff} with increasing energy E_0, as expected, but for $a=10$ Å the behavior is quite different. Here the bulk plasmon is almost independent of energy. The reason for this can be found when the components of K_{eff} are considered.

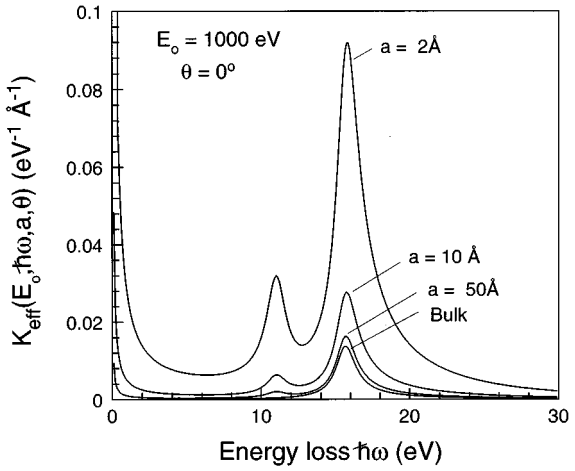

FIG. 3. The dependence of K_{eff} on the depth of excitation for fixed energy $E_0=1000$ eV and exit angle $\theta=0°$. The depths $a=2$, 10, and 50 Å were considered. In addition the figure includes the corresponding bulk inelastic cross section as calculated from Eq. (1).

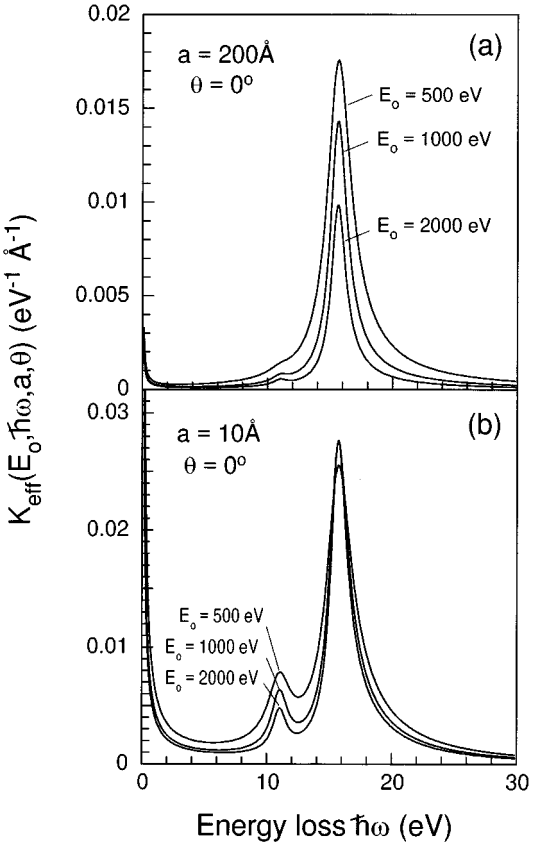

FIG. 4. The energy dependence of K_{eff} with depth of excitation and exit angle fixed at $a=200$ Å and $\theta=0°$. The energies $E_0=500$, 1000, and 2000 eV were considered (a). The equivalent figure when the depth of excitation is changed to $a=10$ Å (b).

In Fig. 5 the calculation has been divided into two contributions, where (a) ''electron contribution'' is a calculation without the hole, and (b) ''hole contribution'' is the difference between a full calculation and the ''electron contribution,'' which corresponds to the effect of the hole. Note that this division is artificial since none of the two contributions corresponds to the physical situation, but it helps the understanding of the behavior in Fig. 4. The cross section that one obtains when the hole contribution is removed corresponds to the situation where an electron is suddenly created without a hole state. This is different from the situation in EELS experiments where the electron moves into the sample and out again. The two situations can therefore not be compared. The energy dependence of the ''electron contribution'' is similar to that of Fig. 4(a). However, the hole contribution to the plasmon intensity increases with increasing energy and saturates for $E_0\gtrsim 2000$ eV. This is expected for the following reason: in the limit of large electron velocity the electron has, within the relaxation time of the plasmon, moved a large distance compared with the wavelength of the typical plasmon. Then the potential changes abruptly (within the relaxation time of the plasmon) and the probability for plasmon excitation is large. For small E_0 we approach the adiabatic limit where the potential around the hole changes more slowly and the probability for excitations is small. The sum of the two contributions [Fig. 4(b)] gives the total effective cross section K_{eff}, where the bulk plasmon is almost inde-

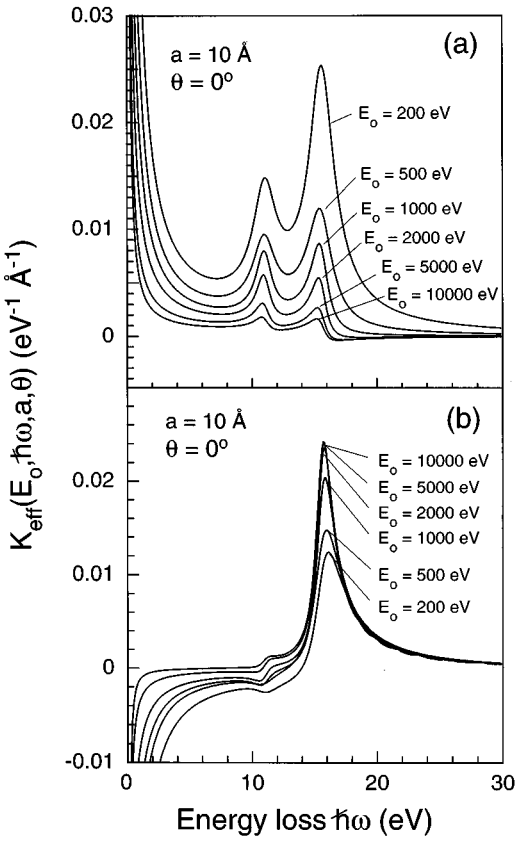

FIG. 5. Energy dependence of the ''electron contribution'' (a) and the ''hole contribution'' (b) (see text for definition). The excitation depth and exit angle are fixed at $a=10$ Å and $\theta=0°$. The energies $E_0=200$, 500, 1000, 2000, 5000, and 10 000 eV were considered.

pendent of energy and the surface plasmon decreases with increasing energy. At $a=200$ Å [Fig. 4(a)] the relative weight of the ''hole contribution'' is so small that the energy dependence of K_{eff} is essentially as in Fig. 5(a).

The present model has the property that $K_{\text{eff}}\rightarrow\infty$ for $\hbar\omega\rightarrow 0$. This is not observed in the REELS model[4,5] and must, consequently, relate to the sudden creation of the electron hole pair at $t=0$. Thus, it describes the well-known skewed elastic peak shape observed in photoemission.[11,12,16,17] The assertion that intrinsic processes are responsible for the singularity in K_{eff} is supported by the fact that the tail is less prominent when long pathlengths are considered (Figs. 2 and 3). That is, the relative weight of extrinsic losses grows.

Figure 6 shows the dependence of $K_{\text{sc}}(E_0,\hbar\omega,\theta)$ on the exit angle θ, for fixed energy $E_0=1413.5$ eV corresponding to the Al $2p$ peak excited with Al $K\alpha$ radiation. The overall trend is that the ratio of the surface to bulk plasmon intensity increases when the exit angles increases.

Figure 7 gives the energy dependence of $K_{\text{sc}}(E_0,\hbar\omega,\theta)$ for fixed exit angle $\theta=0°$. As expected, the surface to bulk plasmon ratio decreases with increasing energy, and the area below the curve decreases with increasing energy.

Figure 8 demonstrates how the core hole contributes to the energy loss. The figure gives K_{sc} for $E_0=1413.5$ eV and $\theta=0°$, together with its two components corresponding to the hole and the electron. From the figure it can be concluded

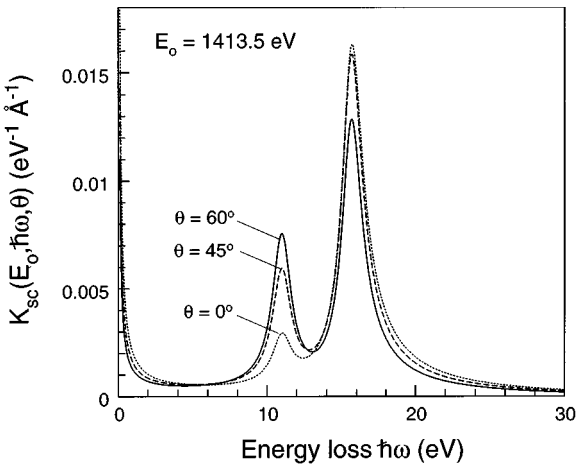

FIG. 6. Dependence of the path length integrated cross section K_{sc} [Eq. (18)] on exit angle. The energy was fixed at $E_0=1413.5$ eV corresponding to Al $2p$ excited with Al $K\alpha$ radiation. The angles $\theta=0°$, 45°, and 60° were considered. The value of the inelastic mean free path was $\lambda=25.4$ Å (Ref. 14).

that the hole gives rise to approximately 50% of the bulk plasmon loss, but contributes little to the surface plasmon intensity. For comparison, experiments have previously shown that intrinsic excitations contribute by $\sim\frac{1}{3}$ to the intensity in the plasmon peak.[18,19] Thus the assumption made by Chen and Chen[9] of neglecting the effect of the core hole cannot be justified by the present model or by experiments. Notice further that the hole component has a negative low-loss tail that is compensated by a positive tail from the electron component, and K_{sc} is positive everywhere as expected.

In Fig. 9, a comparison is made between model spectra calculated according to Eq. (19) and experimental XPS spectra of the Al $2p$ line. The full width at half maximum of the primary line shape $F(E)$ in the model calculation was determined from the experiment. As previously noted we can only compare with experiment in the region corresponding to one inelastic scattering event. The experimental data in (a) and (b), which were taken from Baird *et al.*,[20] explores the exit

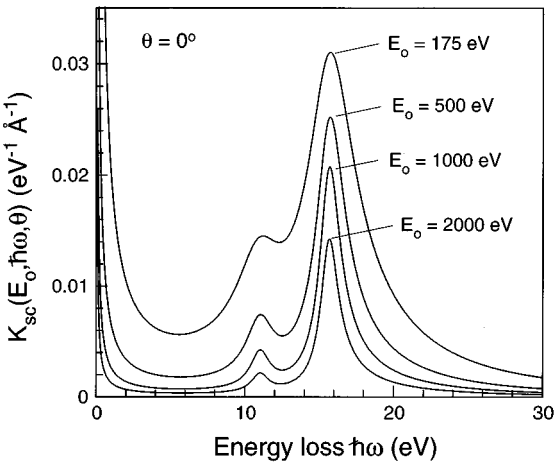

FIG. 7. Energy dependence of K_{sc} for fixed exit angle $\theta=0°$. The following energies and corresponding inelastic mean free paths were considered: $E_0=175$ eV ($\lambda=6.2$ Å), 500 eV ($\lambda=11.5$ Å), 1000 eV ($\lambda=19.4$ Å), 2000 eV ($\lambda=33.9$ Å).

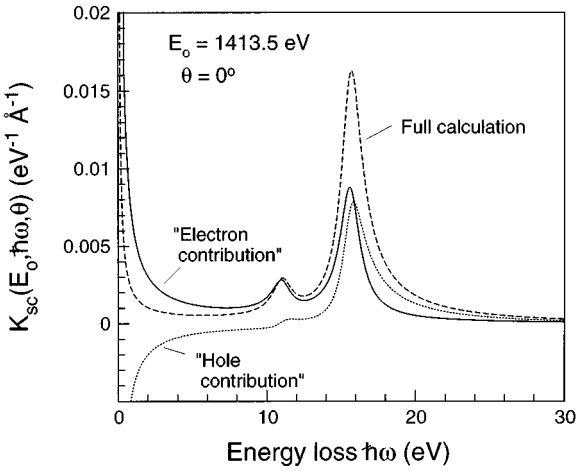

FIG. 8. The K_{sc} cross section at $E_0=1413.5$ eV and $\theta=0°$. The figure shows the full calculation and its two components, the ''electron contribution'' and the ''hole contribution'' (see text for definition). The sum of the two contributions gives the full calculation result.

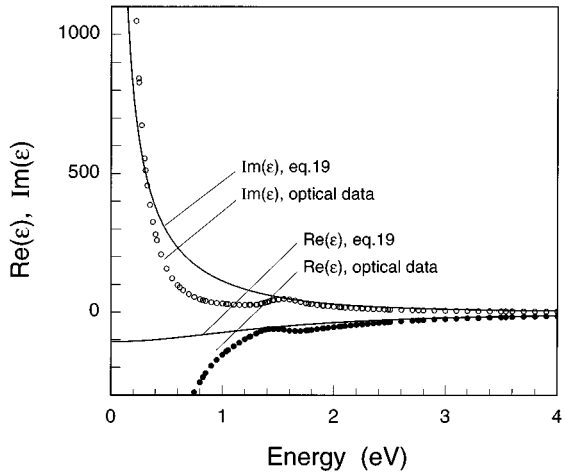

FIG. 10. The real and imaginary parts of the dielectric function for $k=0$. Full lines represents data calculated from Eq. (20) and filled and empty circles are data from optical measurements (Ref. 22).

angle dependence of the losses. The elastic peak energy E_0 is 1413.5 eV corresponding to excitation with Al $K\alpha$ radiation. The surface to bulk plasmon ratio is well reproduced for $\theta=0°$, but at $\theta=60°$ the model exaggerates the surface plasmon intensity. This discrepancy might be due to unwanted effects in the experiment such as roughening and/or oxidation. Furthermore the model assumes that the dielectric function goes abruptly from $\epsilon(\mathbf{k},\omega)$ to 1 at $r_\perp=0$. This is not very realistic and might give too strong a surface plasmon.[20]

The experimental spectrum in Fig. 9(c) was taken with synchrotron radiation at $h\nu=250$ eV ($E_0=175$ eV) and $\theta=0°$.[21] Comparison with the model calculation shows that even for this low energy the model reproduces the correct surface to bulk plasmon ratio. The convolution in Eq. (19) involves integration over a diverging function $[F(E')K_{sc}(E'-E,\hbar\omega,\theta)$ for $E'-E]$ and in fact it turns out that the integral itself diverges (the elastic peak grows without limit). For this reason the integral in Eq. (19) was calculated from $E+0.05$ eV and not from E. The sensitivity towards the chosen cutoff was small and the same cutoff energy was used for all calculations. The deficiency is most probably due to the assumed functional shape of $\epsilon(\mathbf{k},\omega)$ for ω close to zero, which is not accurately described by Eq. (20). This is illustrated in Fig. 10 where the dielectric function in Eq. (20) ($k=0$) is compared with dielectric data obtained from optical measurements.[22] It is clear that the dielectric function in Eq. (20) fails to agree with the optical data below an energy of 2–3 eV. Despite this limitation the model has correctly reproduced the ratio of the elastic peak intensity to the plasmon loss intensity for all three cases (a), (b), and (c) in Fig. 9.

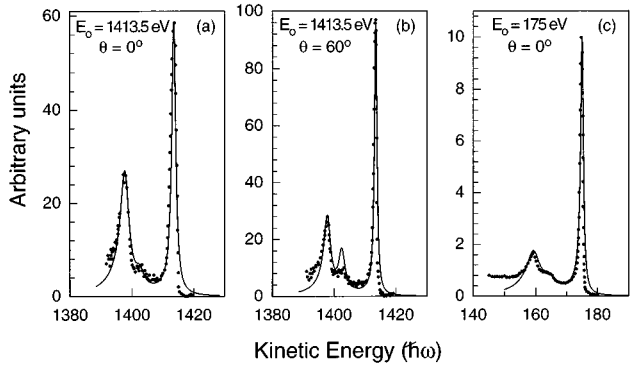

FIG. 9. Comparison of experimental XPS spectra of the Al $2p$ line (dots) and the corresponding model spectra calculated according to Eq. (19) (full line). Experimental data in (a) and (b) are taken from Baird *et al.* (Ref. 20) and have an elastic peak energy of 1413.5 eV and exit angles 0° and 60°, respectively. Data in (c) are taken from Ref. 21 and have elastic peak energy of 175 eV and 0° exit angle.

IV. CONCLUSION

A model to describe electron energy loss in XPS experiments is developed. The procedure is analogous to a previous model for REELS, which was successful in predicting effective inelastic electron cross sections. For a given XPS geometry and primary electron energy, the effective inelastic cross section is determined. It includes the effect of the core hole and, by application of the proper boundary conditions, also surface effects. A systematic study of K_{eff} for aluminum metal reveals that the relative weight of surface loss features is enhanced for glancing emission angles and shallow excitation depths. Furthermore, the energy dependence of K_{eff} is strongly affected by the contribution of the core hole to the energy loss. For increasing primary energy the core hole contributes increasing energy loss. This contribution saturates above a certain energy. The path length integrated cross section [Eq. (18)] is used for evaluation of model spectra corresponding to one inelastic scattering event. Comparison with experimental XPS of Al $2p$ shows good agreement for $\theta=0°$ at $E_0=1413.4$ eV and 175 eV, but for $\theta=60°$ the model overestimates surface losses. The cross section can be resolved into components corresponding to losses produced by the hole and by the electron itself. For Al $2p$ at $\theta=0°$ this analysis shows that the hole contributes approximately 50% to the first bulk plasmon excitation.

[1] J. Lindhard, K. Dan. Vidensk. Selsk. Mat. Fys. Medd. **28**, 8 (1954).
[2] R. H. Ritchie, Phys. Rev. **106**, 874 (1957).
[3] F. Yubero and S. Tougaard, Surf. Interface Anal. **19**, 269 (1992).
[4] F. Yubero and S. Tougaard, Phys. Rev. B **46**, 2486 (1992).
[5] F. Yubero, J. M. Sanz, B. Ramskov, and S. Tougaard, Phys. Rev. B **53**, 9719 (1996).
[6] F. Yubero, D. Fujita, B. Ramskov, and S. Tougaard, Phys. Rev. B **53**, 9728 (1996).
[7] J. L. Gervasoni and N. R. Arista, Surf. Sci. **260**, 329 (1992).
[8] D. L. Seymour, C. F. McConville, D. P. Woodruff, and J. E. Inglesfield, Surf. Sci. **214**, 57 (1989).
[9] Y. F. Chen and Y. T. Chen, Phys. Rev. B **53**, 4980 (1996).
[10] R. H. Ritchie and A. L. Marusak, Surf. Sci. **4**, 234 (1966).
[11] P. H. Citrin, G. K. Wertheim, and Y. Baer, Phys. Rev. B **16**, 4256 (1977).
[12] P. Steiner, H. Höchst, and S. Hüfner, Z. Phys. B **30**, 129 (1978).
[13] Sven Tougaard and Peter Sigmund, Phys. Rev. B **25**, 4452 (1982).
[14] S. Tanuma, C. J. Powell, and D. R. Penn, Surf. Interface Anal. **11**, 577 (1988).
[15] R. H. Ritchie and A. Howie, Philos. Mag. **36**, 463 (1977).
[16] S. Doniach and M. Šunjic, J. Phys. C **3**, 285 (1970).
[17] G. D. Mahan, Phys. Rev. B **11**, 4814 (1975).
[18] S. Tougaard, Phys. Rev. B **34**, 6779 (1986).
[19] D. R. Penn, Phys. Rev. Lett. **40**, 568 (1978).
[20] R. J. Baird, C. S. Fadley, S. M. Goldberg, P. J. Feibelman, and M. Šunjic, Surf. Sci. **72**, 495 (1978).
[21] S. Tougaard, Surf. Interface Anal. **11**, 453 (1988).
[22] *Handbook of Optical Constants of Solids*, edited by Edward D. Palik (Academic, New York, 1985), Vol 1.